precursor for a range of nitrogen ceramic phases, and further ^{15}N NMR studies on these compounds will resolve some of the remaining questions concerning these structures.

Acknowledgment. M.J.L. is grateful to the U.K. Science and Engineering Research Council for a Research Studentship under the Earmarked Scheme. We thank P. Wilson for technical assistance.

Incommensurate Modulations in the Pb-Doped BiSrCaCuO 221 Superconducting Phase: A Five-Dimensional Superspace Description

Yan Gao, Peter Lee, Heinz Graafsma, James Yeh, Peter Bush, Vaclav Petricek,† and Philip Coppens*

Chemistry Department and Institute on Superconductivity, State University of New York at Buffalo, Buffalo, New York 14214

Received January 26, 1990

The new modulation introduced by Pb doping of the 221 BiSrCaCuO superconducting phase has been analyzed by using five-dimensional superspace group theory. The complete X-ray diffraction pattern has monoclinic rather than orthorhombic symmetry and is in agreement with the superspace group $P{:}Aa{:}P1$. In addition to the original modulation with $\mathbf{q}_1 = 0.234\ (1)\mathbf{a}^*$, an extra set of satellites with $q_2 = 0.144\ (3)\mathbf{a}^*$, and "combination" satellites with $q_1 - q_2 = 0.090\ (1)\mathbf{a}^*$ occur. The two modulations differ in the internal translational symmetry. Anomalous dispersion experiments show that both Bi and Pb atoms are affected by each of the modulations, a conclusion confirmed by the diffraction analysis. The displacements of the new modulation are in-phase, rather than out-of-phase, for two adjacent BiO layers. The c-axis displacements of the Bi atoms for the original modulations are significantly reduced, while the amplitudes of the $\mathbf{q}_2$ modulation in this direction exceed 0.3 Å for several of the atoms.

Introduction

The incommensurate modulations in the BiSrCaCu oxides represent structural features that perturb the three-dimensional lattice property of the crystalline materials. As a result their crystal structures cannot be fully described by conventional crystallography. In previous single-crystal studies, we have analyzed the modulations in the 2212 and 221 BiSrCaCuO structures,[1-3] using superspace symmetry theory as developed by De Wolff[4] and De Wolff, et al.[5] The analysis shows displacements of the atoms from their average positions, which are as large as 0.5 Å in the a and c directions of the unit cell. The displacements affect the geometry of all layers in the crystals, including the CuO_2 layers, the geometry of which is crucial for the superconductivity mechanism. Recent studies of commensurate analogues containing Fe and Co rather than Cu are in agreement with the results of our supersymmetry analysis of the superconducting phases and give evidence for the existence of extra oxygen atoms in the Bi–O layers.[6]

As lead doping tends to stabilize the higher T_c phases, the structural details of the lead-doped phases are of importance. The doping also has a dramatic effect on the satellite reflection pattern. As reported,[7-10] Pb doping of the BiSrCaCu oxides induces a second modulation wave in the crystals. In the Ca-containing 221 phase this wave has a modulation vector $\mathbf{q}_2 = 0.144\mathbf{a}^*$, in addition to the modulation with $\mathbf{q}_1 = 0.234\mathbf{a}^*$, which is similar to the undoped 2212 modulation (Table I). It is noteworthy that the modulations in both the undoped and Pb-doped 221 phases are strongly affected by the presence of Ca. The calcium-free Pb-doped 221 sample does not show any satellite reflections in its single-crystal diffraction pattern, as observed by Torardi et al.[11] and confirmed in our experiments. Ramesh et al.[7] report that in the Pb-doped 2223 phase, the 2212-like modulation disappears upon cooling to 88 K while the second modulation is not affected.

Table I. Modulation Wave Vectors for the (Bi and Pb-Doped Bi) 2212 and 221 Phases

phase	wave vector	ref
Bi-2212	$0.210a^*$	1, 2
Bi-221	$0.213a^* + 0.61c^*$	1, 2
Pb-doped Bi-2212	$0.220a^*$ ($\mathbf{q}_1$)	16
	$0.136a^*$ ($\mathbf{q}_2$)	
Pb-doped Bi-221	$0.234\ (1)a^*$ ($\mathbf{q}_1$)	this work
	$0.144\ (3)a^*$ ($\mathbf{q}_2$)	
	$0.090\ (1)a^*$ ($\mathbf{q}_1$–$\mathbf{q}_2$)	

In this paper, we describe an X-ray single-crystal analysis of the two-dimensional modulated structure of the Pb-doped 221 superconductor using the five-dimensional superspace approach. The average structure of the 221

† Permanent address: Institute of Physics, Czechoslovak Academy of Sciences, Na Slovance 2, 180 40 Praha 8, Czechoslovakia.

(1) Coppens, P.; Gao, Y.; Lee, P.; Graafsma, H.; Ye, J.; Bush, P. *Proceedings of Third Annual Conference on Superconductivity and Applications, Buffalo, N.Y.*; Plenum: New York, in press.
(2) Gao, Y.; Lee, P.; Coppens, P.; Subramanian, M. A.; Sleight, A. W. *Science* **1988**, *241*, 954.
(3) Gao, Y.; Lee, P.; Ye, J.; Bush, P.; Petricek, V.; Coppens, P. *Phys. C* **1989**, *160*, 431.
(4) De Wolff, P. M. *Acta* Crystallogr. **1974**, *A30*, 777.
(5) De Wolff, P. M.; Janssen, T.; Janner, A. *Acta Crystallogr.* **1981**, *A37*, 625.
(6) Lepage, Y.; McKinnon, W. R.; Tarascon, J.-M.; Barboux, P. *Phys. Rev.* **1989**, *B40*, 6810.
(7) Ramesh, R.; van Tendeloo, G.; Thomas, G.; Green, S. M.; Luo, H. L. *Appl. Phys. Lett.* **1988**, *53*, 2220.
(8) Chen, C. H.; Werder, D. J.; Espinosa, G. P.; Copper, A. S. *Phys. Rev.* **1989**, *B39*, 4686.
(9) Werder, D. J.; Chen, C. H.; Jin, S.; Sherwood, R. C. *J. Mater. Res.* **1989**, *4*, 748.
(10) Schneck, J.; Pierre, L.; Toledano, J. C.; Daguet, C. *Phys. Rev.* **1989**, *B13*, 9624.
(11) Torardi, C. C. Private Communication, 1989.

0897-4756/90/2802-0323$02.50/0

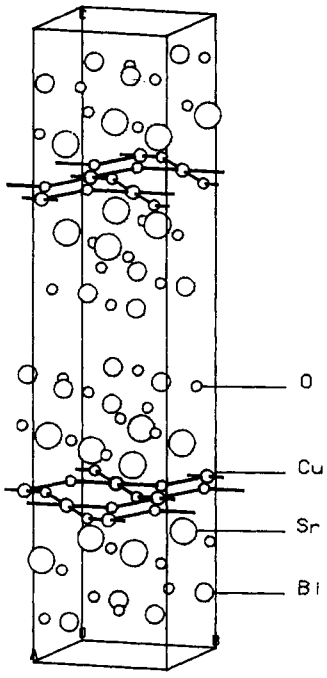

Figure 1. Packing diagram of the 221 phase.

phase is illustrated in Figure 1. Unlike electron-transmission microscopy the X-ray diffraction technique gives an average over the whole sample crystal. The homogeneity of the sample was therefore carefully checked by a series of EDX analyses and by scanning electron microscopy. The single-phase nature of the sample was further confirmed by the absence of any additional diffraction features. It may be noted that this does not exclude the presence of stacking faults in small regions of the crystal. The kinematical theory of diffraction on which structure analysis is commonly based does in fact assume that crystals are not perfect but composed of mosaic blocks bounded by imperfections.

The observation by Y. Ikeda et al.[12] that $\mathbf{q}_1$ satellites occur for Bi-rich (Pb-poor) specimens and $\mathbf{q}_2$ satellites for Pb-rich (Bi-poor) crystals would suggest that the former satellites are due mainly to Bi, and the latter to Pb displacements and/or vacancies. To test this hypothesis independent of the subsequent structure analysis, we measured a number of satellite reflections at both sides of the Bi and Pb L_{III} absorption edges.

Finally, as Ramesh et al. have reported[7] that the $\mathbf{q}_1$ satellite reflections in the Pb-doped 2223 phase slowly disappear at 88 K, variable-temperature measurements of the single-crystal satellite intensities were made covering the 300–20 K range.

Superspace Description of Modulated Crystals

The common definition of a crystal is based on its three-dimensional periodicity, with a unit pattern being repeated at constant intervals in each of three noncoplanar directions, much like the two-dimensional analogue of a wallpaper pattern. Incommensurately modulated crystals do not conform to this definition, because at least in one direction the periodicity is removed by the superposition of a wave with a repeat that is not a simple multiple of the basic translation of the lattice in that direction. The modulation wave may correspond to a displacement of the atoms (a "displacive modulation"), or to nonrandom substitution by a different atomic species (a "substitutional modulation").

In either case a distortion can be described by a plane wave, with wave vector $\mathbf{q}$, such that points at positions defined by the vector $\mathbf{r}$ have identical displacements (respective substitutions) when $\mathbf{q}\cdot\mathbf{r}$ is the same. For a displacive modulation with a sinusoidal displacement wave, the displacement $\mathbf{u}$ of atom ν at $\mathbf{r}_\nu$ is the sum of the contributions of two waves with 0 and 90° phase, respectively:[13]

$$\mathbf{u}_\nu = \mathbf{U}_\nu^x \sin(2\pi\mathbf{q}\cdot\mathbf{r}_\nu) + \mathbf{U}_\nu^y \cos(2\pi\mathbf{q}\cdot\mathbf{r}_\nu)$$

In addition to such a sinusoidal wave higher harmonic waves with a smaller repeat distance are often necessary to describe a modulation.

It was pointed out by De Wolff[4] and by Janner and Jannsen[14] that an incommensurately modulated crystal can still be described as a regularly repeating pattern, if the modulation wave is assumed to be in an extra dimension perpendicular to three-dimensional space. For each different $\mathbf{q}$ vector one such extra dimension is needed. Together they constitute the *internal* space of the crystal. A one-dimensionaly modulated crystal is thus described in four-dimensional superspace, while a crystal with two modulation vectors, as reported here, is described in five-dimensional space. Just as the diffraction pattern of a conventional crystal is the Fourier transform of its three-dimensional structure, the diffraction pattern of the modulated crystal can be considered as the Fourier transform of the $(3 + n)$ dimensional superspace, with the satellite reflections occurring in the extra dimensions. It must be noted that the $(3 + n)$ dimensional space is a convenient mathematical construction; the real structure is the three-dimensional section of this space defined by the *external* dimensions.

Analytical expressions for the intensity of the satellite reflections[13] have been incorporated in a refinement program JANA5,[15] used in the present analysis.

Table II. Atomic Composition of the Single-Crystal Sample, As Measured with EDX[a]

atom	A	B	C	D	E	F	av
Bi	46.4	45.1	45.6	45.3	44.2	43.0	45.0
Pb	4.0	4.2	4.0	4.3	4.0	3.6	4.0
Sr	21.2	21.8	21.7	22.5	21.4	20.6	21.5
Ca	6.9	8.0	7.9	7.1	9.5	11.7	8.5
Cu	21.3	20.9	20.8	20.9	20.9	21.1	21.0

[a] Values given are at different points on the crystal; sampling spot size is 1 μm.

Experimental Section

Sample Preparation and EDX Measurements. The sample was prepared by reacting Bi_2O_3, PbO, $SrCO_3$, CaO, and CuO in the atom ratio Bi:Pb:Sr:Ca:Cu = 1.75:0.25:1.5:2.0:4.5, at 800 °C for 2–3 h. The calcined material was pulverized and heated to 1025 °C in air at a rate of 100 °C/h; it was maintained at this temperature for 14 h. The melt was slowly cooled (20 °C/h) to 920 °C, kept at this temperature for 16 h, cooled (15 °C/h) to 850 °C, and then kept at this temperature for 24 h under O_2 atmosphere. It was then cooled (60 °C/h) to 400 °C and kept at this temperature for 12 h. Platelike single crystals were observed after cooling (200 °C/h) of the bulk to room temperature.

A crystal of dimensions 0.10 × 0.28 × 0.01 mm was selected for analysis. Table II gives the composition at different locations

(12) Ikeda, Y.; Takano, M.; Hiroi, Z.; Oda, K.; Kitaguchi, H.; Takada, J.; Miura, Y.; Takeda, Y.; Yamamoto, O.; Mazaki, H. *Jpn. J. Appl. Phys.* **1988**, *27*, L2067.

(13) Petricek, V.; Coppens P.; Becker P. *Acta Crystallogr.* **1985**, *A41*, 478.

(14) Janner, A.; Janssen, T. *Phys. Rev.* **1977**, *B15*, 643.

(15) Petricek, V.; Coppens, P. *Acta Crystallogr.* **1988**, *A44*, 235.

Table III. Summary of Crystallographic Information

a, Å	5.3312 (6)	no. of reflns coll	4885
b, Å	5.3686 (4)	no. of octants coll	hkl, $hk\text{-}l$
c, Å	24.365 (6)	θ limit, deg	$\theta < 60$
α, deg	90.03 (1)	abs coeff, cm^{-1}	1287.5
β, deg	89.99 (1)	transmission factor	0.015–0.321
γ, deg	89.97 (1)	formula units per cell	4

(sampling size 1 μm) on the crystal as measured by EDX. The experimental composition averaged over these measurements is Bi:Pb:Sr:Ca:Cu = 2.14 (5):0.19 (1):1.02 (3):0.4 (1):1 where the Cu occupancy is normalized, and the standard deviations in brackets are derived from the spread of the measurements. The Sr/Ca content is deficient, as observed earlier for the 2212 and undoped 221 samples. As noted by Cheetham et al.,[16] the cation concentration is closely related to the hole concentration in the CuO plane. The Pb percentage is 8% of the total Bi and Pb content in the sample, which is slightly lower than the Pb percentage found in the homogeneous part of the polycrystalline bulk of our preparation (about 9%) and much lower that of the starting materials (13%). A similar observation was reported by S. Ikeda et al.,[17] who found that for the 2223 phase a ratio of Pb/(Pb + Bi) = 0.20 in the starting material led to a relative Pb content of 0.14 in the final product.

Room-Temperature Diffraction Measurements. Three-dimensional diffraction data were collected with graphite-monochromatized Cu Kα radiation on a CAD4 diffractometer. The choice of Cu Kα (λ = 1.542 Å) was dictated by the need to avoid overlap of the main and the satellite reflections. This was especially important for the $\mathbf{q}_2$ satellites. Cell dimensions were determined from 25 reflections with $30 < \theta < 65°$, giving an orthorhombic average structure. The modulation vectors determined by careful centering of 22 satellite reflections are listed in Table I, while the primary crystallographic information is summarized in Table III.

Variable-Temperature Measurements. To investigate if the modulations disappear at low temperatures, as reported for the 2223 phase, the crystal was mounted on a Huber four-circle diffractometer equipped with a Displex cryostat. The sample was cooled from room temperature to 20 K at a rate of 1 K/min. At 10 K intervals the temperature was maintained for 1 h. During this period, a main reflection (0,0,8,0,0) and two strong satellites (2,0,1,1,0) and (0,0,16,0,1) were measured. Except for an increase in intensity attributable to a reduction in the temperature factor, no significant change in intensity was observed. The experiment was repeated for the Pb-doped 2212 crystal, the structure of which was studied in a separate investigation.[18] Again no disappearance of the satellites was observed. Thus, the disappearance of the $\mathbf{q}_1$ satellites, if confirmed, appears to be unique for the Pb-doped 2223 phase.

Anomalous Scattering Experiment. In an earlier study we used the tunability of the synchrotron source to study the Bi distribution in the 2212 phase with the selective atom diffraction technique.[19] The same method was applied to the Pb-doped 221 single crystal using facilities at the SUNY X3 beamline at the National Synchrotron Light Source. We measured 73 reflections, including 18 main reflections, 22 $\mathbf{q}_1$ satellites, 20 $\mathbf{q}_2$ satellites, and 13 $\mathbf{q}_1$–$\mathbf{q}_2$ satellites, at the wavelengths of 0.924 (on the Bi absorption edge), 0.935 (below the Bi edge), 0.952 (on the Pb absorption edge), and 0.98 Å (below the Pb edge). Each reflection was sequentially measured at the four wavelengths to minimize the effect of source instabilities on the intensities. The ratio between the on-edge intensity and the below-edge intensity of the satellite reflections gives evidence that both Pb and Bi scattering contributes to each of the groups of satellite reflections. This result is in agreement with the subsequent analysis of the conventional diffraction data.

Table IV. Symmetry Operations of the Five-Dimensional Superspace Group

superspace group: P:Aa:$P1$

Symmetry Elements

rotations	translations	rotations	translations
(1,1,1,1,1)	(0,0,0,0,0)	(1,1,1,1,1)	(0,$^1/_2$,$^1/_2$,$^1/_2$,0)
(1,-1,1,1,1)	($^1/_2$,0,0,0,0)	(1,-1,1,1,1)	(0,$^1/_2$,$^1/_2$,$^1/_2$,0)

Table V. Summary of the Refinement

no. of main reflns		249
no. of first-order satellites		1368
no. of second-order satellites		464
no. of variables		142
R/R_W (all)	0.183/0.174	0.148/0.135[a]
R/R_W (main)	0.105/0.117	0.093/0.107
R/R_W ($\mathbf{q}_1$ satellites)	0.200/0.185	0.151/0.145
R/R_W ($\mathbf{q}_2$ satellites)	0.190/0.180	0.180/0.159
R/R_W ($\mathbf{q}_1$–$\mathbf{q}_2$ satellites)	0.285/0.290	

[a] Refinement excluding second-order (combination) satellites.

Table VI. Atomic Parameters of the Basic Crystal Structure[a]

atoms	occupancy	x	y	z
Bi/Pb	1.00	−0.0119 (26)	0.2661 (3)	0.0659 (1)
Sr/Ca	0.77 (1)	0.4897 (26)	0.2470 (5)	0.1784 (2)
Bi/Pb	0.165			
Cu	1.00	0.0000	0.2500	0.2500
O(1)	1.00	0.265 (10)	0.512 (11)	0.249 (1)
O(2)	1.00	0.059 (28)	0.211 (8)	0.149 (4)
O(3)	1.00	0.425 (12)	0.304 (9)	0.071 (3)

atoms	$U(11)$/B_{iso}	$U(22)$	$U(33)$	$U(12)$	$U(13)$	$U(23)$
Bi/Pb	154 (14)	100 (30)	78 (12)	0	0	0
Sr/Ca/Bi/Pb	−1.2 (2)					
Cu	0.2 (3)					
O(1)	3.7 (6)					
O(2)	8.5 (16)					
O(3)	7.7 (17)					

[a] The temperature factor $U(ij)$ is multiplied by 10^4.

Analysis of the Data

Data reduction programs written by Blessing,[20] modified to allow noninteger indexes, were used to derive the structure factors from the intensity data. Absorption corrections were applied with the analytical method.[21] Because of the very high absorption coefficient the accuracy of the absorption correction is affected by surface irregularities of the sample. A total of 2081 main, first-order, and second-order satellite reflections with $I > 3\sigma(I)$ were obtained for use in the refinement.

The extinction rules for the main reflection indicate that the average structure has $A2aa$ or $Amaa$ symmetry. Atomic parameters of the lead-free 221 phase[3] were used as starting values for the refinement. The results of the refinement confirm the noncentrosymmetric space group $A2aa$ for the average structure.

The satellite reflections obey the diffraction condition $k + l + p = 2n$, where p is the fourth index of a reflection $hklpq$. The symmetry of the satellite diffraction pattern indicates the modulations to have monoclinic rather than orthorhombic symmetry. The subgroup Aa, which is also the basic space group of the undoped 221 phase, is in agreement with the experimental information. The symmetry operations of the five-dimensional superspace group are listed in Table IV.

(16) Cheetham, A. K.; Chippindale, A. M.; Hibble, S. J. *Nature* **1988**, *333*, 21.
(17) Ikeda, S.; Aota, K.; Hatano, T.; Ogawa, K. *Jpn. J. Appl. Phys.* **1988**, *27*, L2040.
(18) Lee, P.; Gao, Y.; Yeh, J.; Coppens, P. Unpublished results.
(19) Lee, P.; Gao, Y.; Sheu, H. S.; Petricek, V.; Restori, R.; Coppens, P.; Darovskikh, A.; Phillips, J. C.; Sleight, A. W.; Subramanian, M. A. *Science* **1989**, *244*, 62.
(20) Blessing, R. H. *Crystallogr. Rev.* **1987**, *1*, 3.
(21) Templeton, D. H.; Templeton, L. K. Program AgnostC, University of California at Berkeley, Berkeley, CA, 1978.

Table VII. Atomic Modulation Amplitudes (Å)[a]

atoms	sin components			cos components		
	U_a	U_b	U_c	U_a	U_b	U_c
Bi/Pb(1)						
$\mathbf{q}_1$	0.00 (0)	0.04 (1)	−0.11 (1)	−0.27 (1)	−0.01 (1)	0.00 (0)
$2\mathbf{q}_1$	−0.15 (1)	−0.06 (2)	−0.02 (2)	−0.04 (2)	−0.17 (1)	−0.02 (1)
$\mathbf{q}_2$	0.00 (0)	0.04 (1)	−0.31 (1)	−0.21 (1)	0.00 (1)	0.00 (0)
$2\mathbf{q}_2$	0.01 (1)	0.04 (2)	−0.02 (1)	0.05 (1)	−0.03 (2)	−0.07 (1)
Bi/Pb(2)						
$\mathbf{q}_1$	−0.01 (1)	0.00 (1)	−0.08 (1)	0.15 (1)	−0.00 (1)	−0.02 (1)
$2\mathbf{q}_1$	−0.16 (2)	0.07 (2)	0.00 (2)	0.03 (3)	−0.04 (4)	0.03 (2)
$\mathbf{q}_2$	0.03 (1)	−0.00 (1)	−0.23 (1)	0.14 (1)	−0.00 (1)	0.01 (1)
$2\mathbf{q}_2$	−0.15 (2)	−0.01 (2)	0.02 (1)	−0.03 (2)	−0.03 (2)	−0.14 (1)
Sr/Ca/Bi/Pb(1)						
$\mathbf{q}_1$	−0.04 (1)	−0.02 (1)	−0.15 (1)	−0.18 (1)	−0.05 (1)	−0.02 (1)
$2\mathbf{q}_1$	0.12 (3)	−0.05 (3)	−0.15 (3)	−0.10 (2)	0.18 (2)	−0.20 (2)
$\mathbf{q}_2$	0.12 (1)	0.05 (1)	−0.22 (1)	−0.05 (1)	−0.03 (1)	−0.07 (2)
$2\mathbf{q}_2$	0.10 (3)	0.03 (4)	0.00 (3)	−0.05 (3)	−0.18 (2)	−0.13 (2)
Si/Ca/Bi/Pb(2)						
$\mathbf{q}_1$	−0.02 (1)	0.07 (1)	−0.14 (1)	0.09 (1)	0.02 (1)	−0.01 (1)
$2\mathbf{q}_1$	−0.06 (2)	0.08 (3)	0.23 (2)	−0.03 (3)	0.14 (2)	−0.14 (4)
$\mathbf{q}_2$	−0.07 (1)	−0.01 (1)	−0.32 (1)	0.21 (1)	0.01 (1)	−0.06 (2)
$2\mathbf{q}_2$	−0.06 (2)	0.06 (2)	0.10 (2)	−0.16 (2)	−0.06 (2)	−0.04 (2)
Cu						
$\mathbf{q}_1$	−0.01 (2)	−0.06 (2)	−0.21 (2)	0.02 (3)	−0.03 (2)	−0.03 (3)
$2\mathbf{q}_1$	0.06 (6)	−0.00 (7)	−0.03 (4)	−0.04 (5)	−0.10 (3)	−0.11 (4)
$\mathbf{q}_2$	0.09 (1)	0.00 (1)	−0.35 (1)	0.12 (2)	−0.03 (2)	−0.12 (3)
$2\mathbf{q}_2$	−0.05 (4)	0.03 (4)	0.05 (2)	0.06 (5)	0.01 (6)	−0.02 (3)

[a] The atomic labels 1 and 2 refer to two atomic sites, equivalent in the *A2aa* space group of the average structure, but not equivalent in the basic space group *Aa*.

The average structure was constrained to have *A2aa* symmetry, in accordance with the observed symmetry of the main reflections. Bi/Pb temperature factors were refined anisotropically. As the off-diagonal terms were very small and in one case nonpositive definite, they were fixed to be zero in the final cycles. The remaining temperature factors were refined isotropically, in a refinement that included the main reflections as well as the first- and second-order satellites. The Sr/Ca occupancy of the "Sr" site correlates strongly with the value of the isotropic temperature parameter of the site. The least-squares refinement gives a negative value for this temperature parameter (Table VI). Almost identical R factors are obtained when B_{iso} is fixed at zero; the Sr/Ca occupancy becomes 0.81 (2) instead of 0.77 (2).

Since the scattering powers of Pb and Bi are almost equal for wavelengths not close to an absorption edge, these atoms cannot be distinguished with a conventional X-ray data set. Our previous experience with the 221 phase shows the Sr/Ca ratio to correlate strongly with the cation vacancies in the lattice. Therefore atom-averaged scattering factors were calculated for Bi/Pb (8% of Pb and 92% of Bi) and Sr/Ca (72% of Sr and 28% of Ca) from the atomic ratios as determined by the EDX measurements on the same crystal.

The Cu valency can be calculated from the cation occupancies assuming ideal oxygen composition. The EDX measurements correspond to a formal Cu valency of +2.36, in good agreement with previously reported values for the 2212 phase.[1,2] Our initial refinement with full occupancy at Sr sites led to +1.92 for Cu valency. Therefore, we fixed the Bi/Pb population at the Sr sites at the experimental value of 16.5% derived from the excess Bi/Pb in the crystal as determined by the EDX measurements (Table II), which gives the composition as $Bi_{2.14}Pb_{0.19}Sr_{1.02}Ca_{0.4}Cu$. The subsequent refinement on the total Sr/Ca occupancy of this site leads to a (Sr/Ca + Bi/Pb) occupancy deficiency of 6.5%. The final refinement corresponds to the composition $Bi_{2.14}Pb_{0.19}Sr_{1.11}Ca_{0.43}CuO_6$ and a Cu valency of +2.14. Agreement factors are given in Table V, the atomic positional and temperature parameters in Table VI, and the modulation amplitudes in Table VII. Agreement factors for a refinement excluding the second-order satellites are also listed in Table V. Further treatment may include the oxygen modulation and the (3 + n)-dimensional Bi temperature factor applied in our recent 2212 study.[22]

Discussion

The most important feature of the Pb-doped 221 phase is the occurrence of the new modulation $\mathbf{q}_2$, which differs from the 2212-like $\mathbf{q}_1$ modulation not only in its wavelength but also in the internal translational symmetry (Table IV). The displacements along the a axis for the $\mathbf{q}_2$ modulation wave are illustrated in Figure 2, top. As imposed by the internal symmetry, the c-direction displacements of the $\mathbf{q}_2$ modulation are in-phase for the successive layers in the unit cell (Figure 2, bottom). For this in-phase modulation the interlayer distances between the Bi atoms and the Cu atoms are rather constant instead of varying periodically as in the 2212 phase and in the $\mathbf{q}_1$ modulation in the 221 phase (Figure 3). A similar observation was made recently by Zandbergen et al.[23] using electron microscopy.

The occurrence in the diffraction pattern of numerous rather strong $\mathbf{q}_1$–$\mathbf{q}_2$ satellite reflections suggests that the two modulations occur simultaneously in the microdomains of the crystal. But this would lead to a maximum atomic displacement of 0.7 Å along c for the Cu atoms, which seems unusually large, in particular for an atom that is part of a covalently bonded layer. Chen et al. report that electron transmission lattice images suggest that the $\mathbf{q}_1$ and $\mathbf{q}_2$ modes are spatially separated, but coexist in small regions near the domain boundaries.[8] It is possible that the two waves occur in different microdomains, sufficiently small to give a coherent diffraction pattern including the second-order satellites at $\mathbf{q}_1$–$\mathbf{q}_2$ = 0.09$\mathbf{a}^*$. The improved

(22) Petricek, V.; Gao, Y.; Lee, P.; Coppens, P. *Phys. Rev. B*, in press.
(23) Zandbergen, H. W. Private communication, 1989.

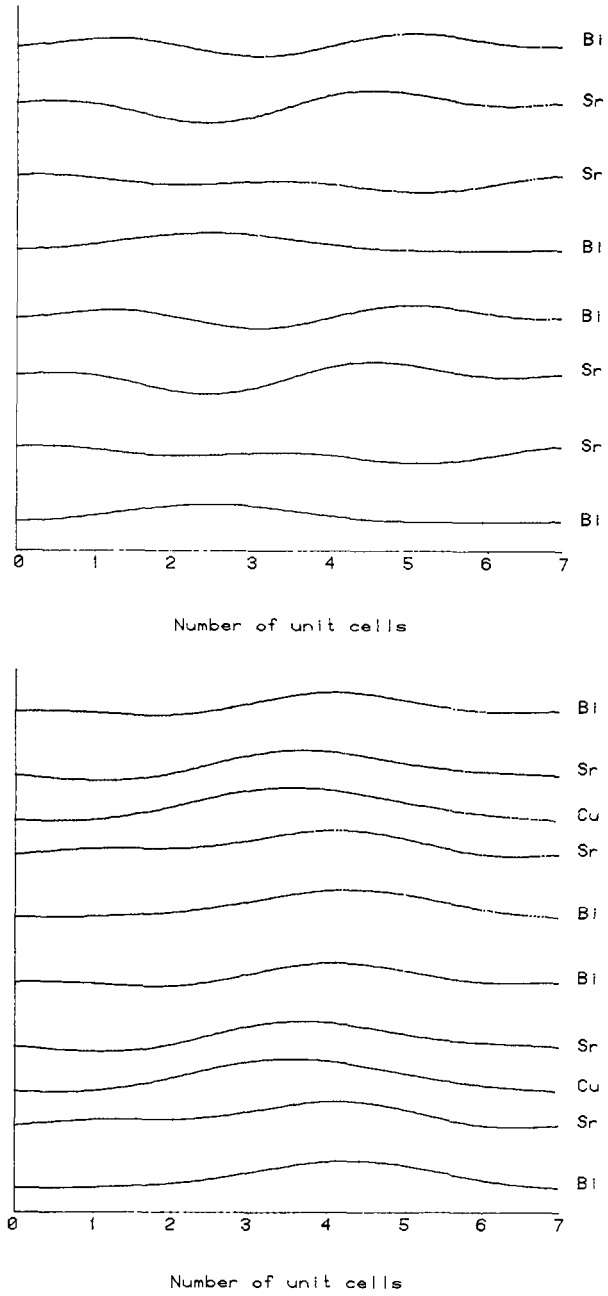

Figure 2. $\mathbf{q}_2$ mode: atomic displacements U, on a relative scale, of successive layers perpendicular to the c axis, which is vertical in the figure. The horizontal axis indicates the number of the unit cell along the a axis. Top: Displacements along a, plotted in the c direction. Bottom: Displacements along c.

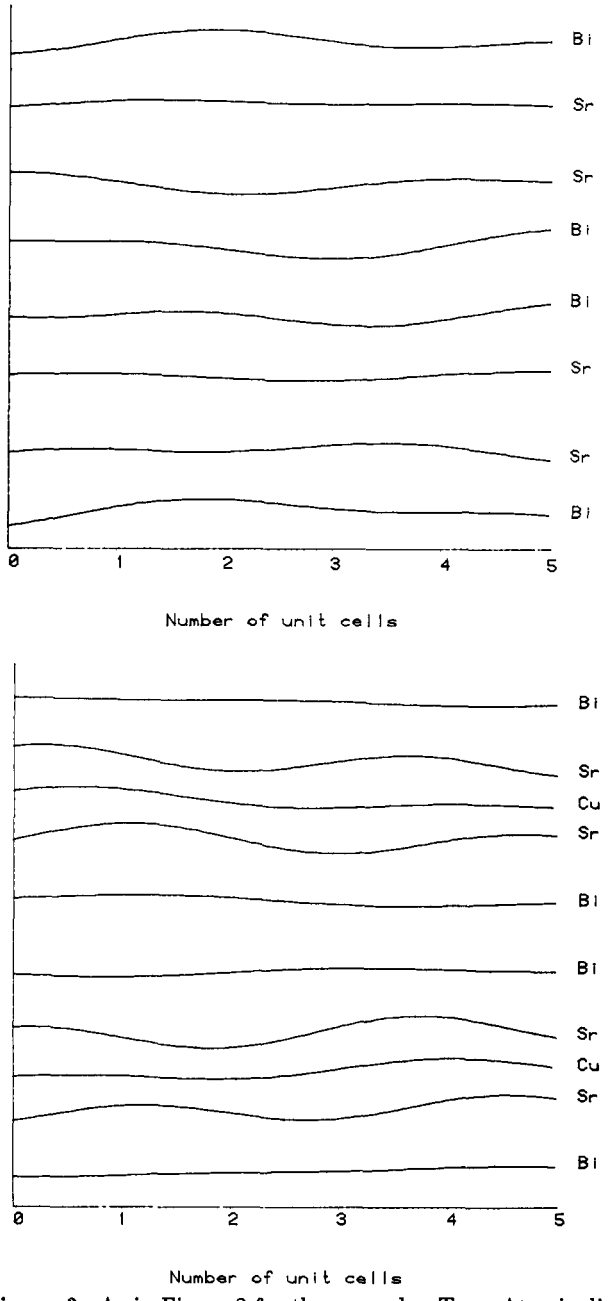

Figure 3. As in Figure 2 for the $\mathbf{q}_1$ mode. Top: Atomic displacements along a. Bottom: Displacements along c.

agreement obtained in the refinement excluding the second-order satellites (Table V) may point in this direction.

While the atomic displacements are primarily within the ac plane, as in the undoped 2212 and 221 phases, some significant contributions along the b direction are observed for the Bi and Sr sites. The displacement amplitudes of the $\mathbf{q}_1$ mode tend to be smaller in the Pb-doped phase; this is especially the case for the Bi displacement along the c direction. Similar weakening of $\mathbf{q}_1$ satellite intensities by Pb doping has been observed in the 2212[24] and 2223[8] phases.

Several mechanisms have been proposed for the origin of the modulation appearing on Pb doping. Ramesh et al. propose that the replacement of Bi^{3+} by Pb^{2+} creates oxygen vacancies or Bi^{5+} ions.[7] The periodic occurrence of such vacancies and substitutions is thought to give rise to the modulation. However, Werder et al.[9] note that increasing Pb content reduces the $\mathbf{q}$ vector, i.e., increases the direct space repeat, and conclude that this is at variance with an explanation based on a repeated vacancy or substitutional defect, because the repeat would decrease with increasing defect concentration. Our analysis shows that the modulation is mainly displacive. However, the displacements may be correlated with Pb/Bi substitution to which the conventional X-ray experiment is not sensitive. The increase of the period on increasing Pb concentration could be a result of the existence of clusters of Pb atoms and oxygen vacancies in the regions of largest displacement, as the clusters would become larger as the lead concentration increases.

Further elucidation of the mechanism of the distortion requires knowledge of the oxygen positions in the modulated structure and the possible preferential Pb/Bi occupancy of specific sites along the modulation vector. We

(24) Lee, P.; Petricek, V.; Gao, Y.; Coppens, P., to be published.

are continuing our anomalous scattering synchrotron experiments at the Pb edge, to investigate the possibility of a substitutional modulation related to the displacement waves described in this report.

Acknowledgment. This work has been supported by the National Science Foundation (CHE8711736) and the New York State Institute on Superconductivity. Synchrotron experiments were performed at the SUNY X3 beamline operated through support of the Division of Basic Energy Sciences of the Department of Energy (DEFG0286ER45231).

Registry No. BiSrCaCuO, 114901-61-0; Pb, 7439-92-1.

Interactions of Water-Soluble Porphyrins and Metalloporphyrins with Smectite Clay Surfaces

Kathleen A. Carrado* and Randall E. Winans

Chemistry Division, Argonne National Laboratory, 9700 S. Cass Ave., Argonne, Illinois 60439

Received December 1, 1989

Two simple water-soluble meso-substituted porphyrins were ion-exchanged into the interlayer space of montmorillonite, hectorite, and fluorhectorite. The porphyrins studied were the chloride salts of tetrakis(1-methyl-4-pyridiniumyl)porphyrin (TMPyP) and tetrakis(*N,N,N*-trimethyl-4-aniliniumyl)porphyrin (TAP) and the corresponding metalloporphyrins Fe^{III}TAP, Fe^{III}TMPyP, and Co^{II}TMPyP. These were ion-exchanged into H-, Li-, Na-, Ca-, Cu-, Co-, VO-, and Fe-montmorillonites and fluorhectorites. The porphyrins are diprotonated in H- and transition-metal-ion-exchanged clays. In group IA and IIA exchanged clays the porphyrins are mainly diprotonated but also exist as free bases. TAP is partially metallated in Cu-montmorillonite. Metalloporphyrin is released into solution after free bases react with Cu- and Co-clays. When metalloporphyrins are ion-exchanged into Ca-montmorillonite and Li-fluorhectorite, stable metalloporphyrin-clay complexes form. TAP and metallo-TAP porphyrins often display larger than expected basal spacings in X-ray diffraction (XRD) spectra that are possibly due to orientation effects. Irreversible changes occur in XRD and UV-visible absorption spectra after heating the porphyrin-clay complexes at only 160 °C.

Introduction

The class of crystalline aluminosilicates with controlled microstructures include zeolites, with pores and channels, and clays, which have two-dimensional layered structures. Within the past few years considerable research has been directed at new uses of such aluminosilicates as advanced materials.[1] Potential applications are based on the ability of these unique structures to selectively incorporate and exchange species within the void spaces on a molecular scale. The conductive properties of zeolites and clays can be altered to allow their use as solid electrolytes, as membranes in ion-selective electrodes, and as host structures for cathode materials in battery systems.[1] Electrode surfaces modified with clays[2] and pillared clays[3] offer both high chemical stability and known and potentially controllable structural features. Studies utilizing zeolite-modified electrodes that interact with water-soluble porphyrins involve photochemical hydrogen evolution,[4] current rectification and electron trapping,[5] and electroassisted catalytic oxidation.[6] However, porphyrin molecules are too large to fit inside the pores and channels of zeolites. Incorporation of porphyrins into the much larger interlayer regions of clays is possible and, in addition, also provides the opportunity of orientation control. The elucidation of the structural organization and photophysical properties of porphyrins in ordered molecular assemblies is a topic of current interest for their use as photoconductors, optical actuators, and chemical sensors.[7]

Smectite clay minerals possess a layered structure where negatively charged silicate layers are separated by positively charged cations and water molecules. The layer charge of such smectites as montmorillonite and fluorhectorite arises mainly from isomorphous substitutions within the middle sheet of the 9.6-Å-thick clay layers. When the charge is compensated for by large inorganic and organic cations in the interlamellar space, the clay sheets are sufficiently separated[8,9] to permit a wide variety of traditional adsorptive and catalytic uses.[10,11] Porphyrins are well-known for both their biological and catalytic properties, and in each case their adsorption by the swelling, layer-lattice silicates is of interest.

This work was undertaken to examine the fundamental interactions of smectite clay surfaces with two cationic, water-soluble porphyrins and their metallo derivatives: the chloride salts of tetrakis(1-methyl-4-pyridiniumyl)-porphyrin (TMPyP) and tetrakis(*N,N,N*-trimethyl-4-aniliniumyl)porphyrin (TAP). Figure 1 shows their structures. The literature to date concerning porphyrin-clay interactions can be divided into two general groups:

* Author to whom all correspondence should be sent.

(1) Ozin, G. A.; Kuperman, A.; Stein, A. *Angew. Chem., Int. Ed. Engl.* **1989**, *28*, 359.
(2) Ege, D.; Ghosh, P. K.; White, J. R.; Equey, J.; Bard, A. J. *J. Am. Chem. Soc.* **1985**, *107*, 5644.
(3) Itaya, K.; Bard, A. J. *J. Phys. Chem.* **1985**, *89*, 5565.
(4) Persaud, L.; Bard, A. J.; Campion, A.; Fox, M. A.; Mallouk, T. E.; Webber, S. E.; White, J. M. *J. Am. Chem. Soc.* **1987**, *109*, 7309.
(5) Li, Z.; Wang, C. M.; Persaud, L.; Mallouk, T. E. *J. Phys. Chem.* **1988**, *92*, 2592.
(6) de Vismes, B.; Bedioui, F.; Devynck, J.; Bied-Charreton, C.; Perree-Fauvet, M. *Nouv. J. Chim.* **1986**, *10*, 81.
(7) Schick, G. A.; Schreiman, I. C.; Wagner, R. W.; Lindsey, J. S.; Bocian, D. F. *J. Am. Chem. Soc.* **1989**, *111*, 1344.
(8) Pinnavaia, T. J. *Science* **1983**, *220*, 365.
(9) Barrer, R. M. *J Inclusion Phenom.* **1986**, *4*, 109.
(10) Odom, I. E. *Philos. Trans. R. Soc. London, A* **1984**, *311*, 391.
(11) Adams, J. M.; Martin, K.; McCabe, R. W. *J. Inclusion Phenom.* **1987**, *5*, 663.

0897-4756/90/2802-0328$02.50/0